ARTICLE

Kinesin-binding protein ensures accurate chromosome segregation by buffering KIF18A and KIF15

Heidi L.H. Malaby[1], Megan E. Dumas[2], Ryoma Ohi[3,4], and Jason Stumpff[1]

Mitotic kinesins must be regulated to ensure a precise balance of spindle forces and accurate segregation of chromosomes into daughter cells. Here, we demonstrate that kinesin-binding protein (KBP) reduces the activity of KIF18A and KIF15 during metaphase. Overexpression of KBP disrupts the movement and alignment of mitotic chromosomes and decreases spindle length, a combination of phenotypes observed in cells deficient for KIF18A and KIF15, respectively. We show through gliding filament and microtubule co-pelleting assays that KBP directly inhibits KIF18A and KIF15 motor activity by preventing microtubule binding. Consistent with these effects, the mitotic localizations of KIF18A and KIF15 are altered by overexpression of KBP. Cells depleted of KBP exhibit lagging chromosomes in anaphase, an effect that is recapitulated by KIF15 and KIF18A overexpression. Based on these data, we propose a model in which KBP acts as a protein buffer in mitosis, protecting cells from excessive KIF18A and KIF15 activity to promote accurate chromosome segregation.

Introduction

Stochastic variations in gene transcription within individual isogenic cells lead to nonuniform protein levels on a cell-to-cell basis (Sigal et al., 2006). These in turn can affect the rate and efficiency of all physiological processes, necessitating counter-measures to buffer the cell against alterations in protein levels that would otherwise be detrimental. Mitosis is particularly sensitive to biological variations in protein expression levels, and abnormally high or low concentrations of mitotic regulators can lead to errors in mitotic spindle function and chromosome segregation. Given the importance of force balance within the mitotic spindle for its assembly and function, it is clear that mechanisms to regulate the activities of molecular motors, such as the mitotic kinesins, would be important for cell division. Indeed, too much or too little mitotic kinesin activity can impair mitotic progression. For example, loss of KIF18A (kinesin-8) function leads to chromosome alignment defects and abnormally long mitotic spindles, whereas cells with increased KIF18A levels form short or multipolar spindles (Mayr et al., 2007; Stumpff et al., 2008; Du et al., 2010). Similarly, increasing or decreasing MCAK (kinesin-13) leads to abnormal chromosome movements and kinetochore–microtubule (MT) attachments (Wordeman et al., 2007). Thus, mitosis requires

regulatory mechanisms that promote optimal levels of motor activity within the spindle.

Sequestration and inactivation of kinesins is one possible mechanism to acutely and reversibly regulate motor activity levels, and kinesin-binding protein (KBP) appears to fulfill this role in at least some cellular contexts. KBP was first identified as a disease-causing gene (dubbed *KIAA1279*) through genetic sequencing of patients with Goldberg–Shprintzen syndrome, a disorder marked by microcephaly, mental retardation, and facial dysmorphism (Brooks et al., 2005; Alves et al., 2010; Drévillon et al., 2013). In neurons, KBP directly inhibits the kinesin-3 family member Kif1Bα, which is necessary for proper mitochondrial transport down the axon (Wozniak et al., 2005). Mitochondrial-derived acetyl-CoA can activate signaling leading to the acetylation of KBP, which is then targeted for degradation, a process linked to decreased mitochondrial biogenesis (Donato et al., 2017). Recently, an extensive biochemical study reported KBP-specific binding to a large panel of human kinesins (Kevenaar et al., 2016). In addition to kinesin-3 family members (KIF1A, KIF1B, KIF1C, and KIF14), KBP was also found to have strong affinity for kinesin-2 family members (KIF3A and KIF3B), kinesin-8 (KIF18A), and kinesin-12

[1]Department of Molecular Physiology and Biophysics, University of Vermont, Burlington, VT; [2]Department of Cell and Developmental Biology, Vanderbilt University Medical School, Nashville, TN; [3]The Life Sciences Institute, University of Michigan Medical School, Ann Arbor, MI; [4]Department of Cell and Developmental Biology, University of Michigan Medical School, Ann Arbor, MI.

Correspondence to Jason Stumpff: jstumpff@uvm.edu; Ryoma Ohi: oryoma@umich.edu.

(KIF15). KBP interacts directly with kinesin motor domains with a 1:1 KBP/motor domain stoichiometry. Motor domain binding by KBP inhibits the kinesin–MT interaction (Kevenaar et al., 2016).

The discovery that KBP binds KIF18A and KIF15 suggests that KBP may also play an important role in regulating cell division, as both of these motors have established mitotic functions. KIF18A localizes to the ends of kinetochore–MTs and confines chromosomes to the spindle equator by regulating kinetochore–MT dynamics (Stumpff et al., 2008; Du et al., 2010). KIF15 maintains spindle integrity by modulating kinetochore–MT separation forces (Tanenbaum et al., 2009; Sturgill and Ohi, 2013). Consistent with a role for KBP in regulating the mitotic functions of KIF15 and KIF18A, it was identified as an interactor of both motors in cycling HeLa cells (Maliga et al., 2013) and has been implicated in regulating KIF15's functions within the spindle (Brouwers et al., 2017).

Here, we establish that KBP inhibits the functions of both KIF18A and KIF15 to promote proper spindle function during mitosis. KBP directly binds the motor domains of KIF18A and KIF15, inhibiting their interactions with MTs. Accordingly, increased expression of KBP, which is primarily cytosolic, disrupts the normal localization of both KIF18A and KIF15 within the spindle. KBP is required to ensure proper chromosome segregation during anaphase, and we show that an excess of either KIF18A or KIF15 results in similar chromosome segregation defects. Based on these data, we propose that KBP functions to buffer kinesin activity during mitosis, ensuring that the activities of KIF15 and KIF18A are maintained within a zone compatible with accurate chromosome segregation.

Results

KBP expression level affects chromosome alignment and spindle length in mitotic cells

To investigate a potential role for KBP during mitosis, we examined KBP's localization and the effects of altering its expression in dividing cells. HeLa and RPE1 cells were transfected with either a control siRNA or a previously described KBP-specific siRNA (Kevenaar et al., 2016; Brouwers et al., 2017). Immunoblotting of cell extracts showed that a specific band near 75 kD was detected with anti-KBP antibodies and that this band was reduced following KBP siRNA treatment (Figs. 1 A and S1). This is consistent with the predicted molecular mass of KBP (72 kD) and previous findings (Wozniak et al., 2005; Drévillon et al., 2013; Kevenaar et al., 2016). Endogenous KBP has been reported to localize to the mitotic spindle in metaphase cells by immunofluorescence (Brouwers et al., 2017). While we also detected spindle staining with an anti-KBP antibody, it was largely unchanged after KBP siRNA treatment in HeLa and RPE1 cells (Fig. S1), suggesting that spindle staining with the KBP antibody is nonspecific. Conversely, an N-terminally mCherry-tagged KBP construct was primarily cytosolic with only faint centrosome and spindle staining (Fig. 1, B and C; and Fig. S1). In interphase cells expressing high levels of mCherry-KBP, KBP was also cytosolic, with occasional puncta colocalizing with MTs (Fig. 1 B, inset). These findings

support previous studies that KBP itself does not exhibit robust MT-binding activity (Kevenaar et al., 2016).

To examine the effects of KBP on early mitotic events, HeLa and RPE1 cells were transfected with either KBP siRNAs or mCherry-KBP, arrested in MG132 to prevent entry into anaphase, fixed, and stained to visualize chromosomes, centromeres, centrosomes, and MTs (Fig. 1 C). Increasing or decreasing KBP levels led to aberrations in chromosome alignment and spindle length in metaphase cells. Chromosome alignment was quantified by measuring centromere distribution along the spindle axis and using the full width at half maximum (FWHM) as a metric for comparison across cell populations and treatment conditions (Stumpff et al., 2012; Kim et al., 2014). KBP siRNA treatment significantly increased the proportion of metaphase cells displaying hyperalignment, characterized by a bilinear arrangement of sister kinetochores at the metaphase plate (Fig. 1 D, middle; and Fig. S2, A and B). Conversely, mCherry-KBP overexpression significantly decreased chromosome alignment. This effect was dose dependent, as chromosome alignment scaled proportionally with mCherry intensity in both HeLa and RPE1 cells (Fig. 1 D, right; and Fig. S2 C). Alterations in KBP expression also affected spindle lengths. KBP siRNA treatment resulted in a population of slightly longer spindles (Figs. 1 E and S2 B). Interestingly, mCherry-KBP overexpression also increased average spindle length, but higher KBP expression led to shorter spindles in both HeLa and RPE1 cells (Figs. 1 E and S2 D). Similar results were obtained in asynchronously dividing HeLa cells that were not treated with MG132 (Fig. S3). Together, these results support a role for KBP in regulating chromosome alignment and spindle length during mitosis.

Codepletion of KIF18A and KIF15 recapitulates the spindle length and chromosome alignment defects seen in KBP-overexpressing cells

KBP was previously identified as a potential interactor of KIF18A, KIF15, and KIF14 from affinity-purification/mass spectrometry analysis of mitotic kinesins (Maliga et al., 2013), and these three mitotic motors were also characterized as KBP substrates by coimmunoprecipitations (coIPs; Kevenaar et al., 2016). While KIF18A's influence of chromosome alignment (Stumpff et al., 2008; Du et al., 2010) and KIF15's effects on spindle length (Tanenbaum et al., 2009; Sturgill and Ohi, 2013) are well established, a role for KIF14 in metaphase has not been documented. KIF14 was cytosolic in metaphase cells and localized to the midbody during telophase (Fig. S4 A). KIF14-specific siRNA treatment significantly reduced KIF14 immunofluorescence but did not detectably affect chromosome alignment or spindle length (Figs. S4, A–C). Therefore, we focused on investigating KIF18A and KIF15 as metaphase KBP substrates.

To determine the effects of KIF18A and KIF15 coinhibition, we knocked down KIF18A, KIF15, or KIF18A and KIF15 using previously validated siRNAs (Stumpff et al., 2008, 2012; Tanenbaum et al., 2009; Sturgill and Ohi, 2013; Kim et al., 2014; Sturgill et al., 2016). Metaphase cells were then fixed and stained to visualize centromeres, centrosomes,
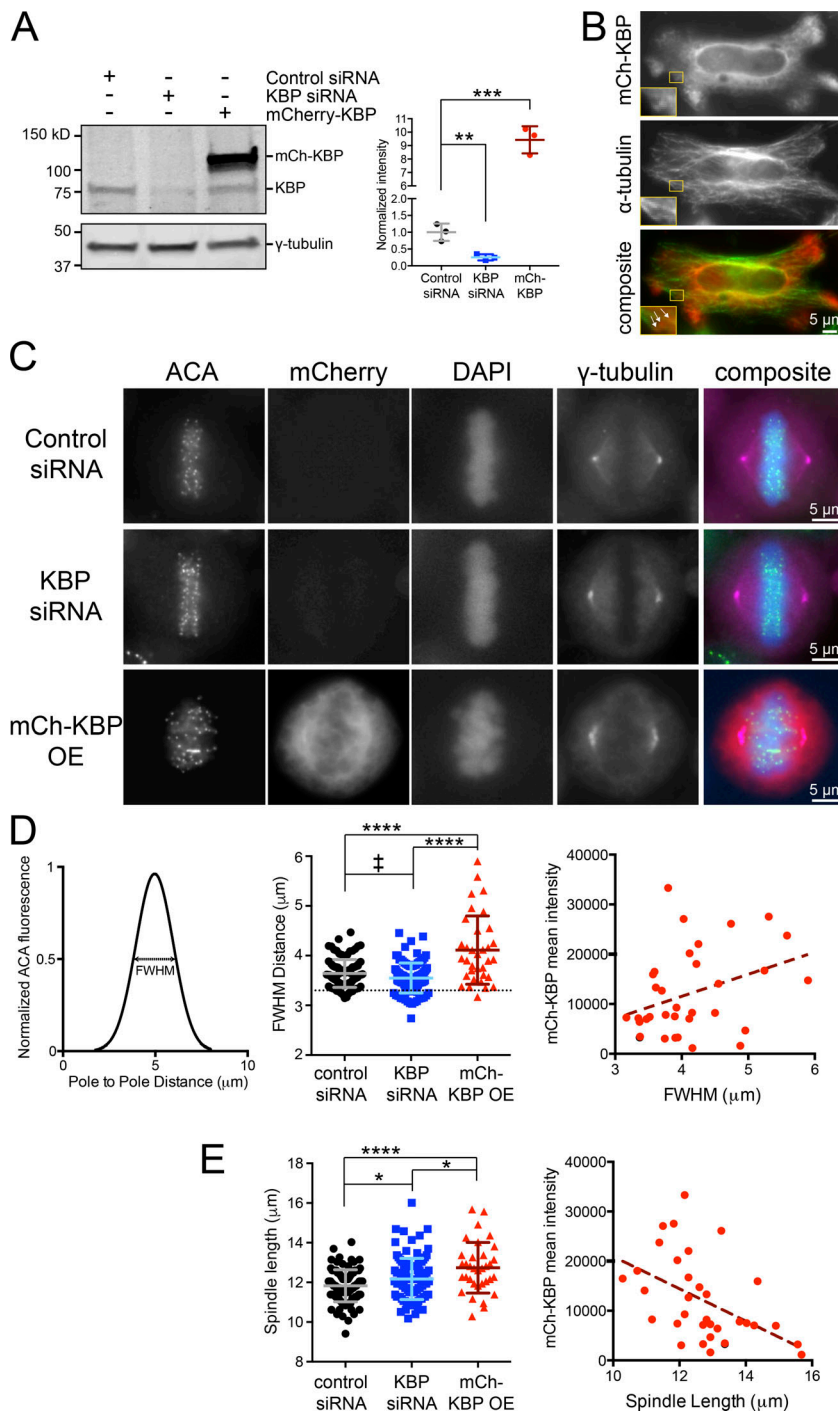
Figure 1. **KBP regulates chromosome alignment and spindle length in mitotic cells. (A)** Western blot against KBP, showing protein levels under KBP siRNA and mCherry-tagged (mCh) KBP transfection conditions from HeLa cells. γ-Tubulin was used as a loading control. Right: KBP knockdown and mCh-KBP overexpression quantification, obtained from quantification of three independent blots, corrected against γ-tubulin and normalized to the control siRNA transfection. **, P = 0.009; ***, P = 0.0002 by unpaired, two-tailed *t* test comparing each condition to control siRNA. **(B)** mCh-KBP does not bind MTs in interphase HeLa cells. Yellow boxes denote inset areas. Arrows highlight occasional mCh-KBP puncta that colocalize with α-tubulin. **(C)** Representative metaphase HeLa cells arrested in MG132 were treated with control or KBP siRNAs or overexpress (OE) mCh-KBP. **(D)** Chromosome alignment was quantified by determining the FWHM of a Gaussian fit to the distribution of ACA fluorescence along the spindle axis. Left: Graphical representation of FWHM measurement. Middle: FWHM distance values for each cell under the indicated conditions. Dotted line denotes cutoff value for hyperaligned cells (3.3 μm), empirically determined from the control population. ‡, P = 0.0432 by χ² analysis comparing hyperaligned populations; ****, adjusted P < 0.0001 with 95% confidence interval by one-way ANOVA analysis with Tukey's multiple comparisons test of full datasets. Right: Correlation plot of mCh-KBP fluorescence intensity versus FWHM alignment values. Dotted line is linear regression showing the data trend. **(E)** Left: Plot of spindle lengths measured in cells following the indicated treatments. *, adjusted P < 0.05; ****, adjusted P < 0.0001 with 95% confidence interval by one-way ANOVA with Tukey's multiple comparisons test. Right: Correlation plot of mCh-KBP fluorescence intensity versus spindle lengths. Dotted line is a linear regression showing the data trend. Error bars represent SD. Data in D and E were obtained from three independent experiments with the following cell numbers: control siRNA (96), KBP siRNA (105), and mCh-KBP OE (34).

chromosomes, and kinesins (Fig. 2, A and B). Chromosome alignment and spindle length were analyzed as in Fig. 1. KIF18A knockdown resulted in unaligned chromosomes (large FWHM values), and this phenotype remained unchanged in combination with KIF15 knockdown (Fig. 2 C, left). This was consistent with our observation that chromosomes align during metaphase in *KIF15Δ*-knockout cells (Sturgill et al., 2016; Fig. S4, D and E). Consistent with previous studies, single KIF18A and KIF15 knockdowns affected spindle length, with the former increasing and the latter decreasing the average distance between spindle poles (Mayr et al., 2007;

Stumpff et al., 2008, 2012; Sturgill and Ohi, 2013; Sturgill et al., 2016; Fig. S4, D and E). Interestingly, HeLa cells codepleted of KIF18A and KIF15 displayed spindle lengths on par with control cells (Fig. 2 C, right). KIF18A and KIF15 depletion was confirmed by immunofluorescence (Fig. 2 D). These results indicate that inhibition of KIF18A and KIF15 in combination could generate the effects observed upon KBP overexpression in Fig. 1. We also note that slightly longer spindle lengths observed in cells at lower mCherry-KBP expression levels could be explained by an increased ability of KBP to inhibit KIF18A compared with KIF15 (Fig. 1 E).
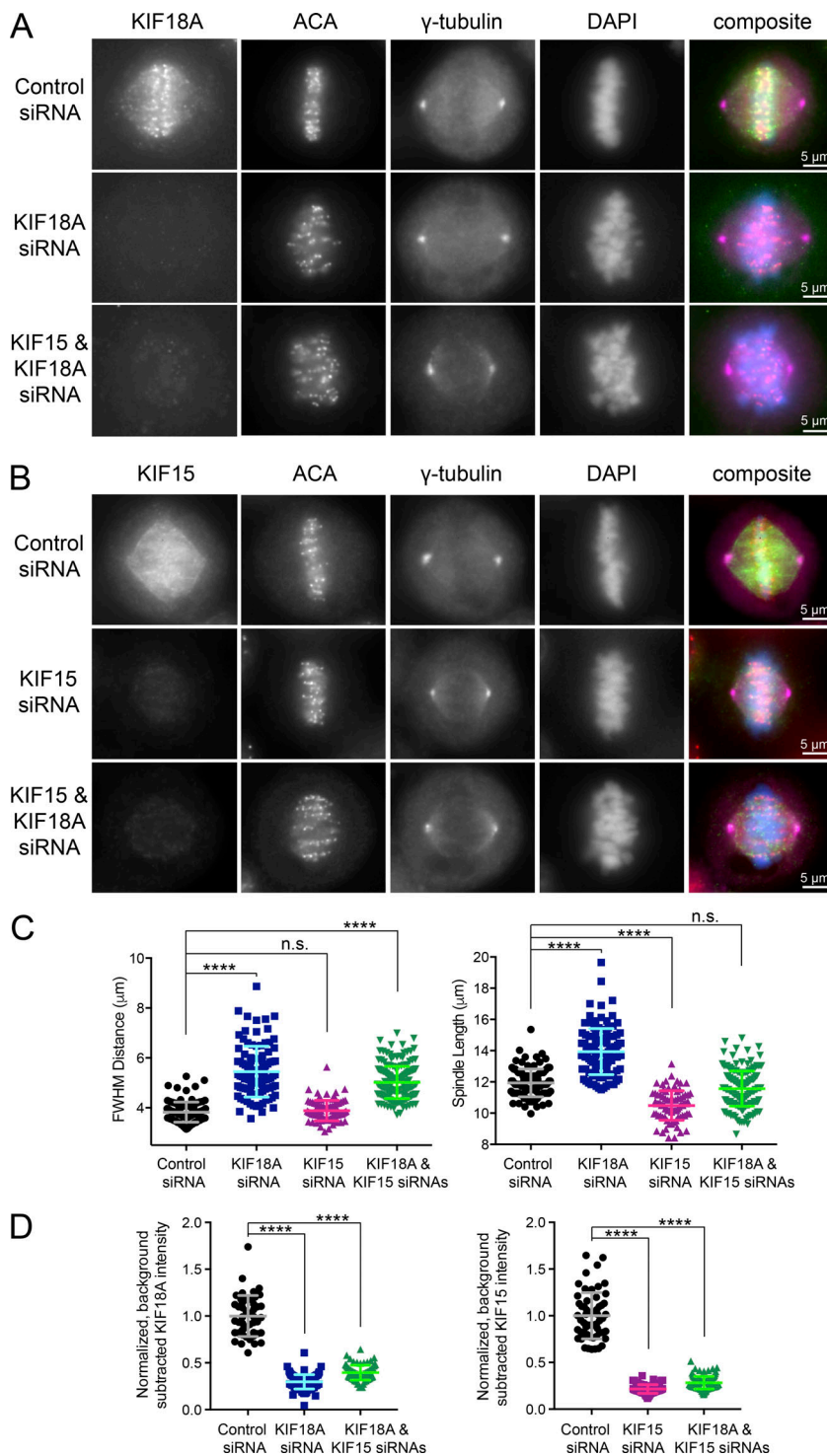
Figure 2. **Metaphase cells deficient in KIF18A and KIF15 display chromosome alignment and spindle length abnormalities. (A and B)** Metaphase cells arrested in MG132 with antibody staining for endogenous KIF18A (A) or endogenous KIF15 (B). **(C)** Quantification of FWHM (left) and spindle length (right) for individual cells treated with the indicated siRNAs. n.s., not significant; ****, adjusted P < 0.0001 with 95% confidence interval by one-way ANOVA with Tukey's multiple comparisons test. **(D)** Quantification of KIF18A (left) and KIF15 (right) knockdown efficiencies for cells analyzed in (C). For the double knockdown quantification, one coverslip each was stained for each kinesin. ****, adjusted P < 0.0001 with 95% confidence interval by one-way ANOVA with Tukey's multiple comparisons test as compared with control siRNA treatment. Error bars represent SD. Data in C and D were obtained from two independent experiments with the following cell numbers: control siRNA (103), KIF18A siRNA (113), KIF15 siRNA (82), and KIF18A and KIF15 siRNA (184).

KBP inhibits KIF18A motor activity more potently than KIF15 motor activity in vitro

To directly measure and compare the effects of KBP on KIF18A and KIF15 activity, C-terminally truncated KIF18A (KIF18A-N480-GFP-His$_6$) and KIF15 (His$_6$-KIF15-N700) were purified from Sf9 cells or Escherichia coli and analyzed via gliding filament assays in the presence and absence of purified GST-KBP (Fig. 3, A and B; Fig. S5, A and B; and Videos 1, 2, 3, and 4). Consistent with previous studies, we found that KBP inhibits the activity of both KIF15 and KIF18A (Kevenaar et al., 2016), and this inhibition occurs in a dose-dependent manner (Fig. 3, A and B), with KIF18A showing enhanced sensitivity to KBP levels (~80% inhibition of KIF18A activity achieved with 100 nM KBP compared with 250 nM KBP for KIF15). Our method of GST-KBP purification yielded protein that eluted as a single peak from a size exclusion chromatography column (Fig. S5). While both gel-filtered and non–gel-filtered GST-KBP were capable of inhibiting motor activity, all data shown are from experiments
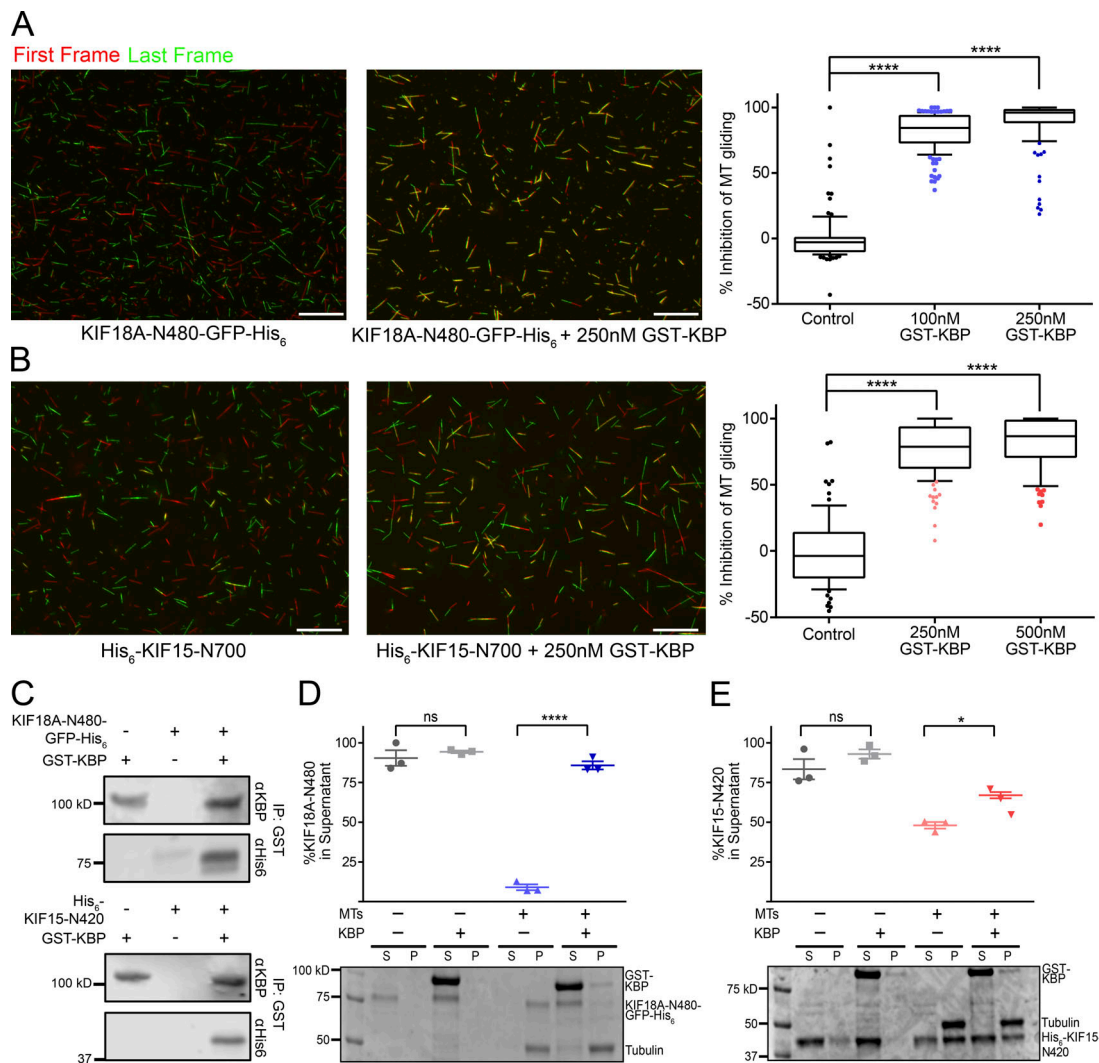
Figure 3. **KBP inhibits KIF15 and KIF18A motor function in vitro. (A)** Gliding filament assay with KIF18A-N480-GFP-His$_6$ and GST-KBP. Left: Representative fields showing the first frame (red) and last frame (green) of MT filaments in the presence or absence of GST-KBP. Scale bars, 20 µm. Full movies (Videos 1 and 2) are available in the online supplemental material. Right: Quantification of percent inhibition of MT gliding for KIF18A-N480-GFP-His$_6$ alone ($n = 95$) or with 100 nM ($n = 147$) or 250 nM ($n = 123$) GST-KBP present in the flow cell. N = total number of MTs measured from triplicate independent experiments. **(B)** Gliding filament assay with His$_6$-KIF15-N700 and GST-KBP. Left: Representative fields showing the first frame (red) and last frame (green) of MT filaments in the presence or absence of GST-KBP. Full movies (Videos 3 and 4) are available in the online supplemental material. Right: Quantification of MT gliding velocity for His$_6$-KIF15-N700 alone ($n = 76$) or with 250 nM ($n = 125$) or 500 nM GST-KBP ($n = 92$) present in the flow cell. N = total number of MTs measured from triplicate independent experiments. Box and whisker plots denote the 10th, 25th, 75th, and 90th percentiles. ****, adjusted P < 0.0001 with 95% confidence interval by one-way ANOVA with Tukey's multiple comparisons test as compared with control gliding reactions. **(C)** Western blot showing coIP of purified 50 nM KIF18A-N480-GFP-His$_6$ (top) or 50 nM His$_6$-KIF15-N420 (bottom) with 250 nM GST-KBP probed with antibodies targeting 6xHis (α His) and KBP (α KBP). **(D and E)** Results of co-pelleting assays for KIF18A-N480-GFP-His$_6$ (D) and His$_6$-KIF15-N420 (E) in the presence and absence of GST-KBP and/or MTs. P, pellet; S, supernatant. Representative Coomassie gels are shown along with quantification of percentage of kinesin motor present in co-pelleting fractions. Data were obtained from three independent experiments. ns, not significant; ****, adjusted P < 0.0001; *, adjusted P = 0.031 with 95% confidence interval by one-way ANOVA with Tukey's multiple comparisons test. Error bars represent SEM.

performed using the more concentrated GST-KBP obtained after single-step glutathione affinity purification.

KBP inhibits MT binding of transport motors such as KIF1A (Kevenaar et al., 2016). To determine if this is also the case for KIF18A and KIF15, we preincubated motors with KBP to allow complex formation and then measured their ability to bind MTs in the presence of AMPPNP. The motor constructs used in these assays (KIF18A-N480-GFP-His$_6$ and His$_6$-KIF15-N420) lacked secondary MT-binding sites outside of the motor domain

(Stumpff et al., 2011; Reinemann et al., 2017), ensuring that any effects of KBP on motor–MT interactions were likely to be mediated through the motor domain. We confirmed that KBP directly associates with both KIF18A-N480 and KIF15-N420 (Fig. 3 C). In the absence of KBP, both KIF18A-N480 and KIF15-N420 co-pelleted with MTs, although with varying efficiencies (Fig. 3, D and E). In the presence of MTs and KBP, both motors shifted from the pellet to the supernatant (>90% for KIF18A and ~20% for KIF15; Fig. 3, D and E). Interestingly, although KBP also

directly binds full-length KIF18A (KIF18A-FL), it does not dramatically reduce the full-length motor's ability to pellet with MTs (Fig. S5, C and E). Consistent with our previous findings showing that KIF15 autoinhibits its ability to bind MTs, KIF15-FL did not interact with MTs in vitro (Sturgill et al., 2014) and also did not bind purified KBP (Fig. S5, D and F). Taken together, these data indicate that KBP directly inhibits KIF18A and KIF15 by blocking the MT binding activity of their motor domains but may not prevent MT interaction when secondary nonmotor MT-binding elements are present.

KBP overexpression alters the spindle localization of KIF18A and KIF15

To determine if KBP alters the interaction of KIF18A and KIF15 with MTs in mitotic cells, we analyzed the localizations of endogenous KIF18A (Fig. 4, A and B) and KIF15 (Fig. 4, C and D) following KBP knockdown or overexpression. KIF18A normally accumulates at kinetochore MT plus ends during metaphase. Measurements of KIF18A distribution along individual kinetochore MT fibers indicated that KIF18A plus-end accumulation was insensitive to KBP knockdown but that the motor showed more uniform spindle distribution following KBP overexpression (Fig. 4 B).

Endogenous KIF15 localizes to MTs throughout the spindle, with a slightly higher concentration observed near the metaphase plate (Fig. 4 C). To quantify changes in KIF15 localization, we determined the width of KIF15's fluorescence distribution along the spindle axis at half of its maximum intensity (FWHM), similar to the metric used to quantify chromosome alignment described in Fig. 1. KIF15 localization was not significantly altered upon KBP knockdown but was distributed more evenly along the spindle in cells overexpressing mCherry-KBP (Fig. 4 D). While endogenous KIF18A accumulation is abolished in even the faintest mCherry-KBP–expressing cells, KIF15 distribution correlates with mCherry-KBP expression level in the cell (Fig. 4 E). Overall, these findings confirm that KBP affects the localization of both KIF18A and KIF15 in mitosis and further support the notion that KBP is a more potent inhibitor of KIF18A than KIF15.

The C termini of KIF18A and KIF15 facilitate spindle localization in the presence of mCherry-KBP

The differential effects of KBP on the MT co-pelleting of KIF18A-FL compared with KIF18A-N480 suggest that the MT-binding site located in KIF18A's C-terminal tail may facilitate MT association in the presence of KBP (Mayr et al., 2011; Stumpff et al., 2011; Weaver et al., 2011). To test whether KIF18A's spindle localization in cells overexpressing KBP depends on its C terminus, we compared the localizations of KIF18A-FL and KIF18A-N480 tagged with GFP (Fig. 5). GFP-KIF18A-FL displayed a more uniform spindle localization and an increase in cytoplasmic motor in the presence of mCherry-KBP (Fig. 5 B). Strikingly, mCherry-KBP expression abolished the spindle localization of GFP-KIF18A-N480, resulting in nearly complete redistribution of the motor to the cytosol (Fig. 5 A and 5B). This finding (1) confirms that KIF18A's C-terminal tail is necessary to maintain MT association when the motor is inhibited by KBP; (2) suggests

that the KIF18A motor domain is unable to associate with MTs when bound to KBP, similar to findings for the kinesin-3 motor KIF1A (Kevenaar et al., 2016); and (3) supports the conclusion that KBP is cytosolic.

KIF15 contains two coiled-coil domains. The C-terminal coiled-coil is responsible for autoinhibition of the motor heads, whereas the proximal coiled-coil displays MT affinity and allows MT cross-linking and sliding in the spindle (Sturgill et al., 2014; Reinemann et al., 2017). Since KBP also alters KIF15 localization within the spindle, we compared the effects of KBP on the spindle localization of KIF15-FL and a truncation mutant (KIF15-N700) containing only the proximal coiled-coil. Surprisingly, GFP-KIF15-FL coexpressed with mCherry-KBP localized stronger to the spindle than GFP-KIF15-FL alone (Fig. 6 B, left) and redistributed closer to the poles (Fig. 6 A), indicating that KBP may alter the equilibrium between the KIF15 autoinhibited and active binding states. GFP-KIF15-N700 displayed weak spindle localization in cells (Fig. 6 A) and became more cytosolic in the presence of mCherry-KBP (Fig. 6 B, middle). Taken together, these results suggest that KIF18A and KIF15 relocalize within the spindle via their C termini when their motor domains are complexed with KBP.

KBP overexpression prevents KIF15-driven spindle stabilization

Given its ability to inhibit the motor activities and mitotic localizations of KIF18A and KIF15, we predicted that KBP would limit the functions of both kinesins in dividing cells. KIF15 has a partially overlapping role with Eg5 in maintaining spindle bipolarity (Tanenbaum et al., 2009) and is essential for bipolar spindle formation when Eg5 is inhibited (Tanenbaum et al., 2009; Sturgill et al., 2016). Thus, to determine the effects of KBP on KIF15's spindle function, we treated cells expressing either mCherry alone or mCherry-KBP with the Eg5 inhibitor S-Trityl-L-cysteine (STLC) or DMSO as a negative control (Fig. 7 A). Fixed metaphase cells were scored for bipolar or monopolar spindles in each treatment condition (Fig. 7 B) and normalized to the DMSO control. Overexpression of mCherry-KBP induced a twofold increase in the number of monopolar spindles, indicating that KBP indeed inhibits KIF15's spindle stabilization function (Fig. 7 C). However, the effect of KBP overexpression was not as severe as complete inhibition of KIF15, which induces monopolar spindles in nearly 100% of mitotic cells in the presence of STLC (Sturgill et al., 2016).

Alteration in KBP expression influences kinetochore oscillations

KIF18A accumulates at kinetochore MT plus ends and suppresses MT dynamics, which contributes to the confinement of chromosomes near the metaphase plate (Stumpff et al., 2008; Du et al., 2010). KIF18A knockdown increases the distance of kinetochores from the metaphase plate and the amplitude of kinetochore oscillations during metaphase, while KIF18A overexpression dampens oscillations (Stumpff et al., 2008). These effects can be assayed by measuring the deviation from the metaphase plate (DMP) and the deviation from average position (DAP) of kinetochores in live metaphase cells (Stumpff
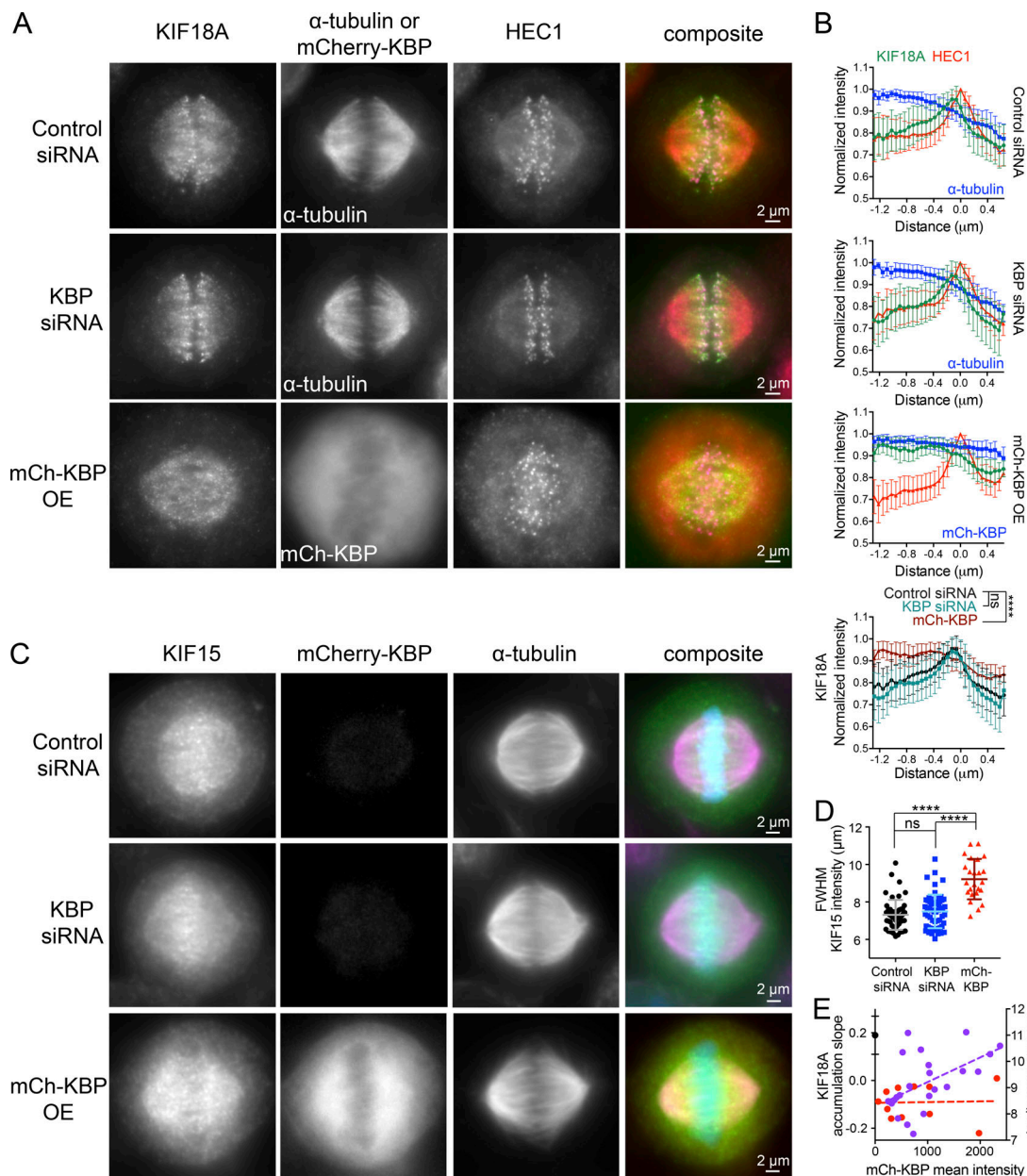
Figure 4. **KBP overexpression alters the localization of both KIF18A and KIF15 on the mitotic spindle. (A)** Localization of endogenous KIF18A in metaphase cells arrested in MG132 after the indicated treatments (OE, overexpression). HEC1 was used as a kinetochore marker. **(B)** Line scans measuring KIF18A distribution along kinetochore MTs. Multiple line scans were averaged after normalizing to peak HEC1 fluorescence intensity. KIF18A, green; HEC1, red; α-tubulin, blue. Solid line indicates the mean, and error bars represent SD. Bottom: Overlay of average KIF18A localization for all three conditions: control siRNA, black; KBP siRNA, blue-green; and mCherry-tagged KBP (mCh-KBP), red. ns, not significant; ****, P < 0.0001 by F-test comparing slopes of linear regressions. **(C)** Localization of endogenous KIF15 in metaphase cells under the indicated treatment conditions. **(D)** Quantification of KIF15 localization on the spindle in cells overexpressing KBP. The FWHM of KIF15 intensity was determined for each cell analyzed. ns, not significant; ****, adjusted P < 0.0001 with 95% confidence interval by one-way ANOVA with Tukey's multiple comparisons test. Error bars represent SD. **(E)** Correlation plot of KIF15 FWHM alignment values (right y axis, purple) and slopes of KIF18A accumulation (left y axis, red) as a function of mCh-KBP fluorescence in individual cells. KIF18A distribution slopes were averaged from two to four line scans per cell. Black dot denotes average KIF18A accumulation slope under control siRNA condition with standard deviation. Dotted lines are a linear regression showing the data trend. Data in B and D obtained from three independent experiments each with the following cell and line scan numbers: (B) control siRNA (21 [61 lines]), KBP siRNA (22 [63 lines]), mCh-KBP OE (19 [53 lines]); (D) control siRNA (51), KBP siRNA (59), and mCh-KBP OE (24).

et al., 2008, 2012). To determine the effects of altered KBP expression on kinetochore oscillations, GFP-CENP-B–expressing cells were transfected with control siRNAs, KBP siRNAs, or plasmids encoding mCherry or mCherry-KBP. Mitotic cells were then imaged using time-lapse microscopy (Videos 5, 6, 7, and 8) and analyzed by tracking GFP-CENP-B–labeled kinetochore pairs. Fig. 8 (A and B) shows representative kinetochore pair tracks and kymographs for all conditions. KBP knockdown
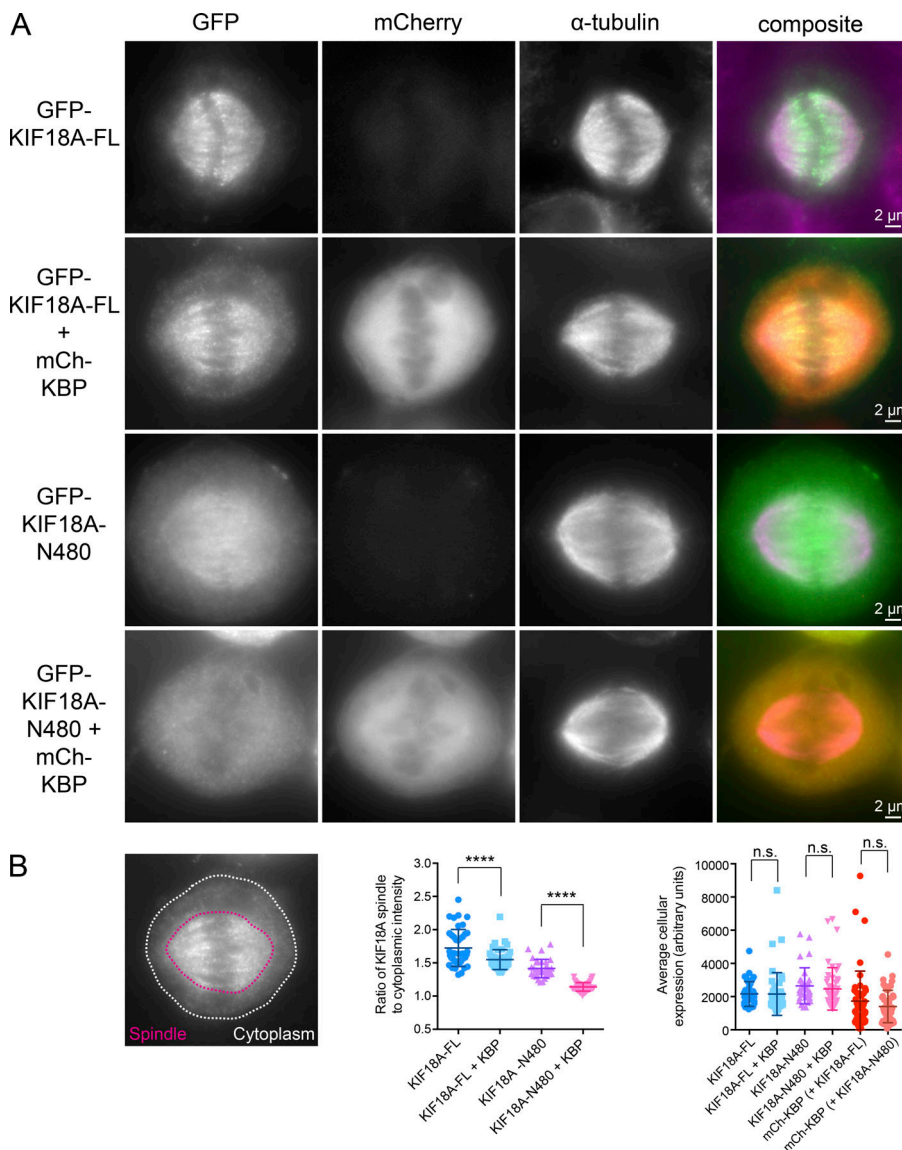
A

Figure 5. **KIF18A's C-terminal tail maintains spindle localization upon KBP overexpression. (A)** Metaphase cells arrested in MG132 transfected with GFP-tagged KIF18A-FL or C-terminally truncated GFP-tagged KIF18A-N480 with or without mCherry-tagged KBP (mCh-KBP). **(B)** Left: Representative image indicating areas used to define spindle (red) and cytoplasmic (white) GFP-KIF18A fluorescence intensity. Middle: Quantification of background subtracted spindle-to-cytoplasmic ratio determined for individual cells in each condition. ****, adjusted P < 0.0001 with 95% confidence interval by one-way ANOVA with Tukey's multiple comparisons test. Right: Quantification of background-subtracted average fluorescence intensity of the indicated constructs; n.s., not significant with 95% confidence interval by one-way ANOVA with Tukey's multiple comparisons test. Error bars represent SD. Data were obtained from three independent datasets with the following cell numbers: GFP-KIF18A-FL (41), GFP-KIF18A-FL + mCh-KBP (47), GFP-KIF18A-N480 (32), and GFP-KIF18A-N480 + mCh-KBP (47).

B

showed a significant reduction in both the DMP and DAP compared with control knockdown cells (Fig. 8 C, black data). In contrast, mCherry-KBP overexpression significantly increased both the DMP and DAP measurements compared with mCherry alone (Fig. 8 C, red data). These results are consistent with KBP inhibiting KIF18A's function in controlling kinetochore oscillations and are in agreement with the measured effects of KBP on chromosome alignment (Figs. 1, S2, and S3).

KBP knockdown or KIF18A/KIF15 overexpression results in lagging chromosomes during anaphase

Our data indicate that KBP limits the activity of KIF18A and KIF15 during mitosis, suggesting that KIF18A and KIF15 hyperactivity could be detrimental to spindle function and chromosome segregation. To test this, we analyzed chromosome segregation following KBP knockdown (Fig. 9 A). KBP depletion led to a twofold increase in anaphase cells with lagging chromosomes compared with controls (Fig. 9 B). Importantly, of the cells that contained lagging chromosomes, those depleted of KBP

exhibited a higher frequency of cells with more than one or two lagging chromosomes (Fig. 9 C). These results show that KBP is required for normal chromosome segregation.

To determine if this phenotype is reflective of excess KIF18A and KIF15 motor activity, we overexpressed mCherry alone, mCherry-tagged KIF18A, GFP-tagged KIF15, or mCherry-tagged KIF18A and GFP-tagged KIF15 in combination (Fig. 9 D). We observed that overexpression of either mCherry-KIF18A or GFP-KIF15 increased the frequency of lagging chromosomes and that the number of lagging chromosomes per cell scaled proportionally with increasing fluorescence intensity (Fig. 9 E). In addition, we found that cells with the highest expression (top 25%) of mCherry-KIF18A or GFP-KIF15 alone or in combination were much more likely to have multipolar spindles in addition to multiple lagging chromosomes, particularly in the double motor overexpression condition (Fig. 9 F). To determine the level of motor overexpression, we labeled mCherry-KIF18A– and GFP-KIF15–expressing cells with antibodies specific to the motors. We found that kinesin levels were increased
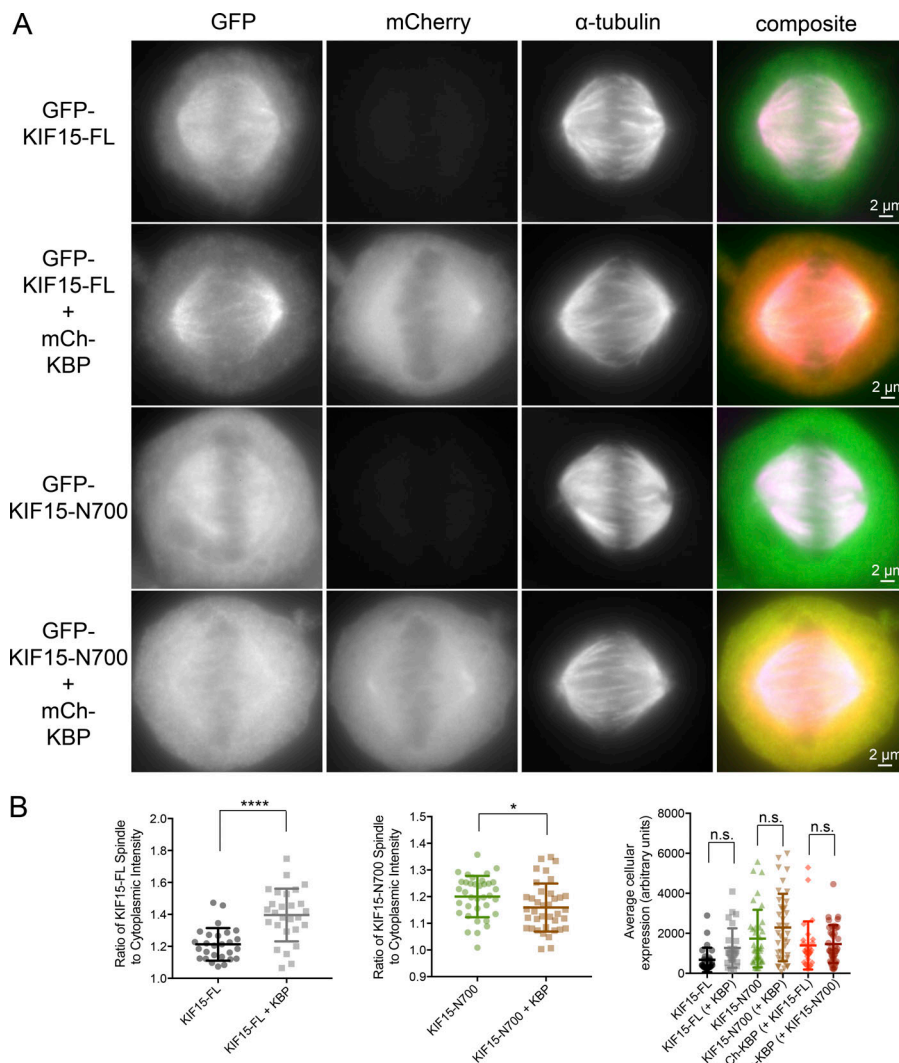
Figure 6. **KIF15's C-terminal tail contributes to spindle localization in the presence of KBP. (A)** Metaphase cells arrested in MG132 transfected with GFP-tagged KIF15-FL or C-terminally truncated GFP-tagged KIF15-N700 with or without mCherry-tagged KBP (mCh-KBP). **(B)** Quantification of background subtracted spindle-to-cytoplasmic ratio of GFP in individual cells expressing GFP-KIF15-FL (left) and GFP-KIF15-N700 (middle). ****, P < 0.0001; *, P = 0.0387 by unpaired, two-tailed *t* test. Right: Quantification of background subtracted average fluorescence intensity of the indicated constructs; n.s., not significant with 95% confidence interval by one-way ANOVA with Tukey's multiple comparisons test. Error bars represent SD. Data were obtained from three independent datasets with the following cell numbers: GFP-KIF15-FL (27), GFP-KIF15-FL + mCh-KBP (27), GFP-KIF15-N700 (36), and GFP-KIF15-N700 + mCh-KBP (38).

~1.5-fold on average compared with controls (Fig. 9 G), a range that is on par with measured protein variations that occur naturally within cell populations (Sigal et al., 2006). Taken together, these results indicate that KBP inhibition of KIF18A and KIF15 is necessary to prevent chromosome segregation errors during anaphase, which can result from relatively modest increases in kinesin levels.

Discussion

Our data indicate that KBP reduces the activities of KIF18A and KIF15 and that this control is required for proper mitotic spindle function and chromosome segregation. In agreement with published work (Kevenaar et al., 2016), we find that KBP blocks KIF18A and KIF15 activity by preventing their catalytic domains from interacting with the MT lattice. Accordingly, altered KBP expression in metaphase cells disrupts chromosome alignment, reduces spindle length, and destabilizes spindle bipolarity. These effects are consistent with inhibition of KIF18A and KIF15 function. The ability of KBP to disrupt motor–MT interactions is also supported by the effects of KBP

overexpression on KIF18A and KIF15 localization. Excess KBP prevents KIF18A from accumulating at kinetochore MT plus ends, instead causing the motor to indiscriminately bind spindle MTs, most likely through a secondary MT-binding site in KIF18A's C-terminal tail (Stumpff et al., 2011). When this region containing this site is removed, both KIF18A and KBP are exclusively cytosolic. Similarly, KBP inhibition of KIF15 causes the motor to adopt a more uniform distribution along the spindle, which depends on the KIF15 C terminus (Sturgill et al., 2014). Phosphorylation has also been shown to alter KBP binding to kinesin motors (Kevenaar et al., 2016), and acetylation of KBP can promote its degradation (Donato et al., 2017), both of which could add to the complexity of KIF18A and KIF15 regulation. Our observation that KIF15-FL localizes more strongly to the spindle when coexpressed with KBP (a finding we are not able to recapitulate in vitro with purified components) also implicates additional modes of regulation between KIF15 and KBP that should be explored in future studies.

Another recent report identified KBP as a regulator of KIF15 in mitotic cells. Our findings, however, contradict some of the primary conclusions of this study (Brouwers et al., 2017).
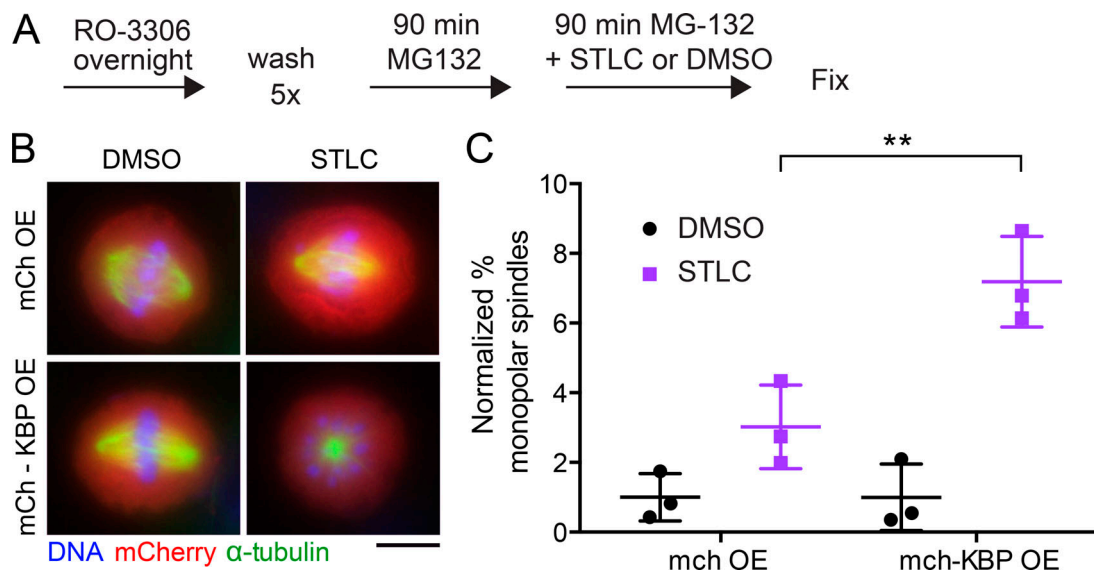
Figure 7. **KBP overexpression inhibits KIF15-driven spindle stabilization. (A)** Schematic of spindle collapse assay. **(B)** Metaphase cells expressing mCherry (mCh) only or mCh-KBP treated with DMSO or the Eg5 inhibitor STLC. Scale bar, 10 μm. **(C)** Quantification of the percentage of mitotic cells with monopolar spindles, normalized to the DMSO condition. Error bars represent SD. Data were obtained from three independent experiments with the following cell numbers: mCh only DMSO (103), mCh only STLC (134), mCh-KBP DMSO (200), and mCh-KBP STLC (269). **, adjusted P = 0.0058 with 95% confidence interval by two-way ANOVA with Tukey's multiple comparisons test.

Brouwers et al. reported that KBP promotes metaphase chromosome alignment by enhancing KIF15 localization near chromosomes and increasing kinetochore–MT stability (Brouwers et al., 2017). In contrast, we found that loss of KBP function leads to hyperalignment of chromosomes, a phenotype consistent with increased KIF18A activity at kinetochore–MT plus ends. Furthermore, our data indicate that KBP reduces the accumulation of KIF15 near the center of the spindle and that chromosomes align during metaphase despite complete loss of KIF15 activity, a conclusion supported by other studies of KIF15 function in mitosis (Sturgill and Ohi, 2013; van Heesbeen et al., 2014). Brouwers et al. also concluded that KBP localizes to the spindle. Evidence presented here and in previous studies (Kevenaar et al., 2016) suggests that KBP does not directly interact with MTs. Our immunofluorescence analyses of endogenous KBP were complicated by nonspecific spindle staining. mCherry-KBP appears to faintly label spindle MTs and centrosomes, but the majority of the protein is cytosolic. Our data are consistent with the conclusion that KBP does not bind MTs directly, but we cannot rule out that a small fraction of the protein localizes to spindles indirectly via kinesins that contain nonmotor MT-binding domains. Along these lines, the infrequent association of KBP with MTs in interphase cells (Fig. 1 B) may be indirect, mediated through kinesin-2 and kinesin-3 motors.

Our finding that KBP has a greater inhibitory effect on KIF18A compared with KIF15 agrees with previous immunoprecipitation assays (Kevenaar et al., 2016). Differential preference for the two motors could explain the range of spindle lengths observed in Fig. 1 E, where KBP overexpression resulted in a cell population with longer spindle lengths on average even though knockdown of KIF18A and

KIF15 in combination produced cells with normal spindle lengths (Fig. 2 C). The longer spindles in cells expressing low levels of mCherry-KBP could be caused by specific inhibition of KIF18A, while the shorter spindles in cells expressing higher levels of mCherry-KBP could result from KIF15 inhibition (Fig. 1 E, right). Interestingly, cells that expressed low levels of exogenous KBP but were not arrested in metaphase did not form long spindles (Fig. S3 B). This result is consistent with increased spindle length in KIF18A knockdown cells depending on mitotic arrest (Mayr et al., 2007). Why might KBP have evolved a higher potency for KIF18A? Our analyses of chromosome segregation suggest that cells are less tolerant of KIF18A overexpression. Therefore, increased specificity of KBP for KIF18A may be necessary to ensure accurate chromosome segregation.

The regulation of both KIF18A and KIF15 by KBP is required to prevent lagging chromosomes in anaphase. Given the multipolar phenotype observed from overexpression of KIF18A and KIF15, it is likely that these lagging chromosomes are caused, at least in part, by merotelic attachments. Merotelic attachments are a common cause of segregation errors, especially when the integrity of the spindle and control of chromosomal oscillations are compromised (Cimini et al., 2001; Bakhoum and Compton, 2012). Other mechanisms such as blocking error correction in kinetochore–MT attachment or linking neighboring kinetochore MTs are also possible (Vladimirou et al., 2013). We have found that our kinesin overexpression assays at most increase the expression of KIF18A and KIF15 by fourfold compared with endogenous levels (Fig. 9 G). However, cells with the highest levels of kinesin expression exhibit multipolar spindles, which were not observed in KBP knockdown cells. Thus, we speculate that cells lacking KBP form bipolar spindles and lagging
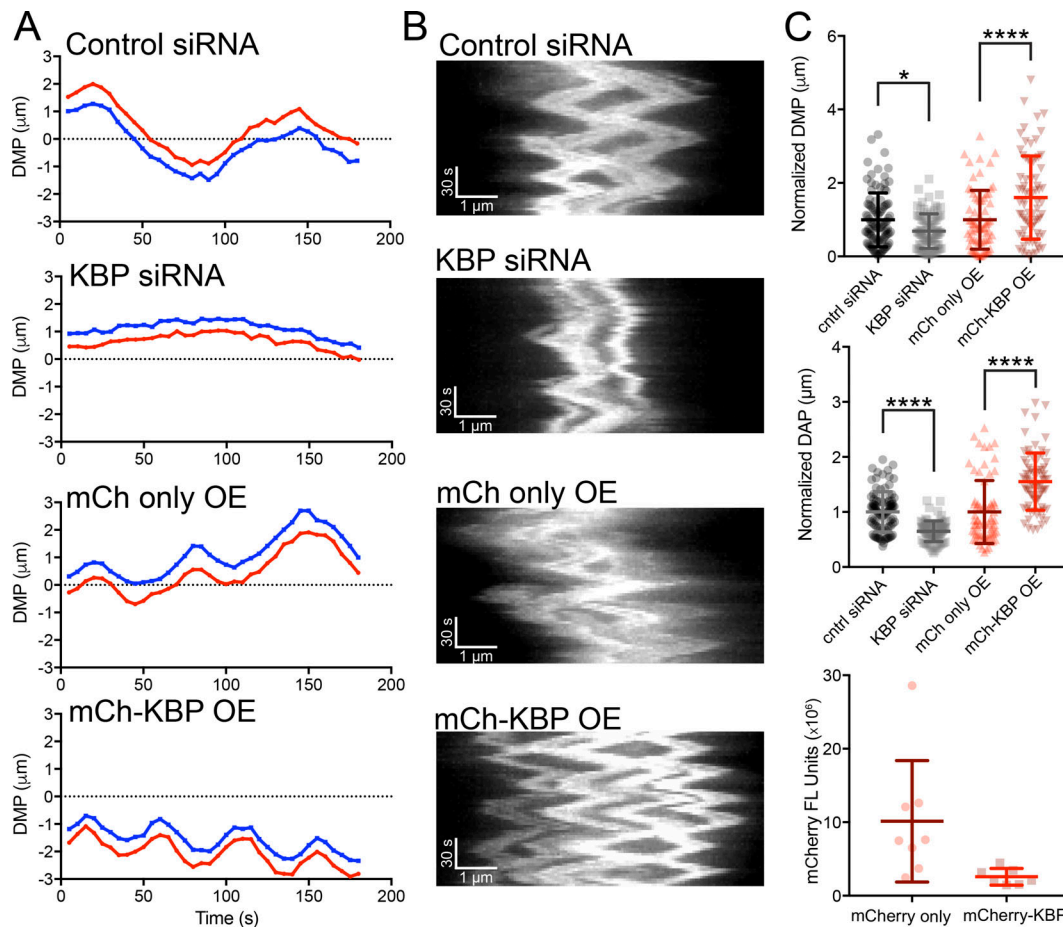
Figure 8. **Altered KBP expression affects kinetochore oscillatory movements. (A)** Example traces showing the movement over time of representative kinetochore pairs relative to the metaphase plate (dotted line) in cells from the indicated experimental conditions. **(B)** Representative kymographs of GFP-tagged CENP-B dynamics in metaphase cells transfected with the indicated siRNAs or plasmids. Full videos (Videos 5, 6, 7, and 8) are available in the online supplemental material. **(C)** Quantification of the DMP, DAP, and mCherry (mCh) fluorescence. DMP and DAP values were normalized to control siRNA or mCh-only conditions. *, adjusted P < 0.05; ****, adjusted P < 0.0001 with 95% confidence interval by one-way ANOVA with Tukey's multiple comparisons test. Error bars represent SD. Data were obtained from the following numbers of cells over two or three independent experiments: control siRNA (10 [97 kinetochores]), KBP siRNA (12 [83 kinetochores]), mCh only (8 [69 kinetochores]), and mCh-KBP (7 [75 kinetochores]). OE, overexpression.

chromosomes due to increases in KIF18A and KIF15 activity that are lower than fourfold.

We propose a model where KBP functions as a protein buffer in the mitotic system, acting through its varying affinity for specific kinesin substrates as a referee to maintain an optimal level of KIF18A and KIF15 motor activity within the spindle. Why would a mode of regulation evolve to inhibit specific kinesin function when there are clearly established modes of transcriptional, translational, and ubiquitin-mediated degradation regulation (Nath et al., 2015)? Precedence for sequestration as a regulatory mechanism has been established for the actin and MT cytoskeletons, as well as enzymes such as cyclin-dependent kinases (Safer et al., 1991; Harper et al., 1993; Xiong et al., 1993; Jourdain et al., 1997). Similar to these systems, the mitotic spindle requires finely balanced control (Prosser and Pelletier, 2017), leaving little wiggle room for variations in activity levels. Protein concentration can vary within a cell population up to 30% and can change significantly over cell generations, as shown by tracking protein expression through

multiple cell divisions (Sigal et al., 2006). While KBP itself would also be subject to this variability, there is already evidence that "excess" KBP (KBP unbound to kinesins) is targeted for degradation by acetylation (Donato et al., 2017). We propose that KBP functions to ensure that minor fluctuations in protein levels do not interfere with these precisely balanced forces, thus promoting robust and reproducible division of genetic material among protein expression variations within cells.

Materials and methods

Plasmids and siRNAs

mCherry-KBP and mCherry-KIF18A were constructed by Gateway Cloning Technology (Thermo Fisher Scientific). First, the KBP gene (HA-KBP plasmid; gift from C. Hoogenraad, Utrecht University, Utrecht, Netherlands; Kevenaar et al., 2016) and KIF18A open reading frames were inserted into pCR8/GW/TOPO (Thermo Fisher Scientific). Correctly inserted clones were confirmed by sequencing. The KBP and KIF18A genes were then
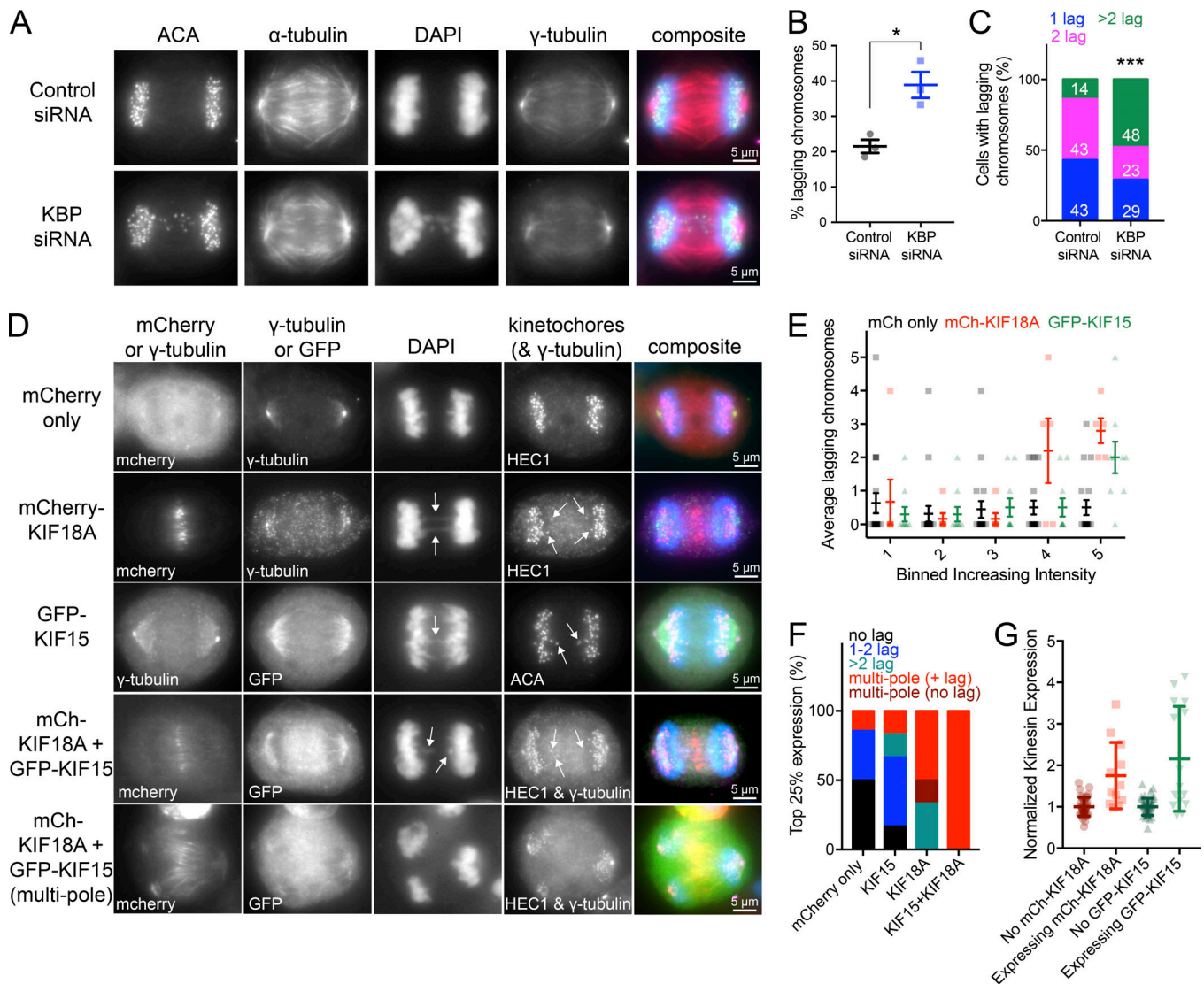
Figure 9. **Cells deficient in KBP or overexpressing KIF18A and/or KIF15 display multiple lagging chromosomes in anaphase. (A)** Anaphase cells treated with control or KBP siRNAs. **(B)** Quantification of the percentage of lagging chromosomes under the two knockdown conditions. *, P = 0.0136 by unpaired, two-tailed t test. Data were obtained from three independent experiments with the following cell numbers: control siRNA (66) and KBP siRNA (82). **(C)** Among the cells with lagging chromosomes, quantification of the number of lagging chromosomes per cell: one lagging chromosome, blue; two lagging chromosomes, pink; and more than two lagging chromosomes, green. White numbers indicate percentage for each group. The number of cells with lagging chromosomes analyzed are as follows: control siRNA (13) and KBP siRNA (31). ***, P < 0.001 by χ^2 analysis. **(D)** Anaphase cells overexpressing either mCherry only, mCherry-KIF18A, GFP-KIF15, or both mCherry-KIF18A and GFP-KIF15. Arrows point to lagging chromosomes. **(E)** Quantification of the average lagging chromosomes in cells as a function of mCherry (mCh) only, mCh-KIF18A, or GFP-KIF15 overexpression level. Background-subtracted fluorescence intensity values were equally divided into bins. Individual data points are shown in the background; foreground shows the average number of lagging chromosomes with SDs. Data were obtained from seven independent experiments with the following cell numbers: mCh only (92), mCh-KIF18A (28), and GFP-KIF15 (49). Bin 4 mCh only versus mCh-KIF18A adjusted P = 0.0044; bin 5 mCh only versus mCh-KIF18A adjusted P < 0.0001; bin 5 mCh only versus GFP-KIF15 adjusted P = 0.0016 with 95% confidence interval by two-way ANOVA with Tukey's multiple comparisons test. **(F)** Breakdown of the number of lagging chromosomes or multipolar spindle phenotypes observed in the 25% highest expressing cells for each condition. No lagging chromosomes, black; one or two lagging chromosomes, blue; more than two lagging chromosomes, green; multipolar spindles with lagging chromosomes, red without lagging chromosomes, dark red. Data were obtained from four independent experiments with the following total cell numbers: mCh only (55), mCh-KIF18A (19), GFP-KIF15 (23), and mCh-KIF18A and GFP-KIF15 (18). P < 0.0001 by χ^2 analysis. **(G)** Normalized kinesin expression levels in anaphase cells. Anaphase cells were imaged and partitioned into either expressing or not expressing mCh/GFP tagged kinesins. Plot displays background-subtracted immunofluorescence levels from KIF18A- or KIF15-specific antibodies normalized to the average from untransfected cells. Average fold increase in kinesin expression above endogenous for each kinesin: mCh-KIF18A (1.75) and GFP-KIF15 (2.16). All error bars represent SD. Data were obtained from two independent datasets with the following cell numbers: KIF18A not expressing mCh-KIF18A (39), KIF18A expressing mCh-KIF18A (12), KIF15 not expressing GFP-KIF15 (46), and KIF15 expressing GFP-KIF15 (15).

inserted by LR recombination reaction (Thermo Fisher Scientific) into a custom Gateway destination vector containing an N-terminal mCherry gene in frame with R1/R2 recombination sites downstream of a cytomegalovirus promoter. Clones were screened by restriction digestion, and the full open reading frames were confirmed by sequencing. For protein expression,

GST-KBP was constructed by isothermal assembly, where the full-length human KBP cDNA (clone 4550085; GE Healthcare) was inserted into the pGEX6P1 vector (Amersham). Clones were screened by Sal1 and EcoR1 digestion and the full open reading frame confirmed by sequencing.

Other constructs used in this study are described elsewhere as follows: GFP-CENP-B (Wordeman et al., 2007), GFP-KIF15 and GFP-KIF15-N700 (Sturgill et al., 2014), GFP-KIF18A-FL and GFP-KIF18A-N480 (Du et al., 2010; Stumpff et al., 2011), and CMV-mCherry alone previously used to clone mCherry-MCAK (Peris et al., 2009). Scrambled control siRNA was obtained from Thermo Fisher Scientific (Silencer Negative Control #2). The KBP siRNA antisense sequence (Kevenaar et al., 2016) was 5′-UAUCAUAGUAAGCAUGUGCUU-3′ (Qiagen), the KIF18A siRNA antisense sequence (Stumpff et al., 2008, 2012; Kim et al., 2014) was 5′-GCUGGAUUUCAUAAAGUGG-3′ (Ambion), and the KIF15 siRNA antisense sequence (Tanenbaum et al., 2009; Sturgill and Ohi, 2013) was 5′-GGACAUAAAUUGCAAAUAC-3′ (Dharmacon). A SMARTpool of four siRNA sequences (Dharmacon) was used to target human KIF14.

Cell culture and transfections

HeLa and RPE1 cells were cultured at 37°C with 5% CO_2 in MEM-α medium (Life Technologies) containing 10% FBS plus 1% penicillin/streptomycin (Gibco). The HeLa KIF15 knockout cell line (Sturgill et al., 2016) was cultured in DMEM (Life Technologies) with the above supplements. For siRNA transfections in a 24-well format, ~80,000 cells in 500 µl MEM-α medium were treated with 35 pmol siRNA and 1.5 µl RNAiMax (Life Technologies) preincubated for 20 min in 62.5 µl OptiMeM (Life Technologies). Cells were treated with siRNAs for 48 h before fixing or imaging. Plasmid transfections were conducted similarly, but with 375 ng kinesin or mCherry-KBP plasmid DNA (100 ng GFP-CENP-B) and 2 µl LTX (Life Technologies). Plasmid transfections were incubated for 24 h before fixing or imaging. Transfections were scaled up by well diameter as needed. For assays with sequential knockdown and plasmid transfections, the media was changed before plasmid transfection mix added.

Western blot analysis

For KBP Western blot detection, ~350,000 cells were plated into a six-well dish and transfected as described above (scaled siRNA: 150 pmol siRNA + 6 µl RNAiMax in 250 µl OptiMeM; scaled plasmid: 1.5 µg plasmid + 8 µl LTX in 250 µl OptiMeM). Cells were washed once in PBS (Thermo Fisher Scientific) and lysed in 200 µl PHEM Lysis Buffer (60 mM Pipes, 10 mM EGTA, 4 mM $MgCl_2$, and 25 mM Hepes, pH 6.9) with 1% Triton X-100 and Halt protease and phosphatase inhibitors (Thermo Fisher Scientific) by scraping the plate and incubating on ice for 10 min. Then lysates were spun at maximum speed for 10 min and 180 µl supernatant added to 60 µl 4× Laemmli buffer prepared with βME (BioRad). Samples were run on precast 4–15% gradient gels (BioRad), transferred to a low-fluorescence polyvinylidene difluoride (PVDF) membrane (BioRad), blocked for 1 h in 1:1 Odyssey blocking buffer (Li-Cor) and TBS (150 mM NaCl and 50 mM Tris base, pH 7.4) + 0.1% Tween-20 (TBST). Primary antibodies against mouse-KBP (1:1,000; H00026128-B01P;

Abnova) and rabbit-γ tubulin (1:1,000; ab11317; Abcam) were added in TBS overnight at 4°C. The membrane was washed with 2× TBST for 5 min each, and then secondary antibodies (goat anti-mouse IgG DyLight 800 conjugate and donkey anti-rabbit IgG DyLight 680 conjugate, both at 1:10,000; SA5-10176 and SA5-10042; Thermo Fisher Scientific) were added in 1:1 Odyssey blocking buffer and TBST for 1 h at room temperature. The membrane was washed with 2× TBST and then 1× TBS for 5 min each and developed on an Odyssey CLx (Li-Cor).

Cell fixation and immunofluorescence

For metaphase observations, cells were treated with 20 µM MG132 (Selleck Chemicals) for 1–2 h before fixation. MG132 treatment is indicated in the figure legends. For spindle collapse assays, cells were collected in G2 overnight with 9 µM RO-3306 (Axxora), washed 5× with DMEM supplemented with FBS and penicillin/streptomycin, and then treated for 90 min with 5 µM MG132, followed by 90 min with 5 µM MG132 + 10 µM DMSO or 10 µM STLC (Sigma-Aldrich). Cells were fixed on coverslips in –20°C methanol (Fisher Scientific) plus 1% paraformaldehyde (Electron Microscopy Sciences) for 10 min on ice, dunked briefly, and then washed three times for 5 min each in TBS. Coverslips were blocked with 20% goat serum in antibody-diluting buffer (Abdil: TBS, pH 7.4, 1% BSA, 0.1% Triton X-100, and 0.1% sodium azide) for 1 h at room temperature before the following primary antibodies diluted in Abdil were added for 1 h at room temperature: mouse anti-α-tubulin at 1 µg/ml (T6199; Sigma-Aldrich), mouse anti-γ-tubulin at 1 µg/ml (T5326; Sigma-Aldrich), rabbit anti-KIF18A at 2 µg/ml (A301-080A; Bethyl), rabbit anti-KIF15 at 1 µg/ml (Sturgill and Ohi, 2013), rabbit anti-GFP at 4 µg/ml (A11122; Molecular Probes), rabbit anti-KIF14 at 2 µg/ml (ab3746; Abcam), and mouse anti-KBP at 1 µg/ml (H00026128-B01P; Abnova). Cells were incubated with the following primary antibodies overnight at 4°C: human anti-centromere antibodies (ACAs) at 2.5 µg/ml (15-235; Antibodies Inc.) and mouse anti-HEC1 at 0.5 µg/ml (GTX70268; GeneTex). All mCherry images are direct measurement of mCherry fluorescence. Incubation with 1 µg/ml goat secondary antibodies against mouse, rabbit, or human IgG conjugated to Alexa Fluor 488, Alexa Fluor 594, or Alexa Fluor 647 (A11029, A11032, A21236, A11034, A11037, A21245, A11013, and A11014; Molecular Probes) occurred for 1 h at room temperature. Two 5-min washes in TBS were performed between rounds of primary and secondary antibody incubations, finishing with three TBS washes before mounting with Prolong Gold anti-fade mounting medium with DAPI (Molecular Probes).

Protein purification

His_6-KIF15-N420, His_6-KIF15-N700, His_6-GFP-KIF15-FL, KIF18A-N480-GFP-His_6, and KIF18A-FL-GFP-His_6 purifications have been described previously (Stumpff et al., 2011; Sturgill et al., 2014; Reinemann et al., 2017).

GST-KBP was expressed in BL21DE3 cells with 0.4 mM IPTG overnight at 16°C. Cells were pelleted and flash frozen in liquid nitrogen and stored at –80°C. For purification, pellets were resuspended in lysis buffer (1× PBS, 500 mM NaCl, 5 mM β-mercaptoethanol [β-ME], 1% NP-40, and protease inhibitors

[Complete Protease Inhibitor Cocktail tablets; Sigma-Aldrich]). Lysate was incubated with 1 mg/ml of lysozyme for 30 min on ice, followed by sonication. Lysate was clarified by centrifugation at 35,000 rpm for 1 h at 4°C in a Ti 45 rotor (Beckman). Clarified supernatant was incubated with 2 ml glutathione-agarose (Sigma-Aldrich) for 1 h at 4°C and washed with ~200 ml wash buffer (1× PBS, 500 mM NaCl, and 5 mM β-ME). Protein was eluted with 1 M Tris (pH 8.0), 3M KCl, and 200 mM glutathione and peak fractions were buffer exchanged into storage buffer (10 mM K-Hepes, pH 7.7, 100 mM KCl, and 1 mM DTT) using a PD 10 desalting column (GE Healthcare). Protein concentration was determined using Bradford assays, and powdered sucrose was added 10% wt/vol before the protein was aliquoted, frozen in liquid nitrogen, and stored in –80°C.

Microscopy

Cells were imaged on a Ti-E inverted microscope (Nikon Instruments) with Nikon objectives Plan Apo λ 60× 1.42 NA and APO 100× 1.49 NA with a Spectra-X light engine (Lumencore) and environmental chamber at 37°C. A Clara cooled charge-coupled device (CCD) camera (Andor) and iXon X3 EMCCD camera (Andor) were used. The Ti-E microscope is driven by NIS Elements software (Nikon Instruments). Gliding filament assays were performed on a Nikon Elements controlled Eclipse 90i (Nikon) equipped with a 60× 1.4 NA (Nikon) objective and a Cool Snap HQ2 CCD camera (Roper). Spindle collapse assay cells were acquired using a 60× 1.4 NA objective (Olympus) on a DeltaVision Elite imaging system (GE Healthcare) equipped with a Cool SnapHQ2 CCD camera (Roper).

Gliding filament assays

Flow chambers were assembled using a glass slide, a smaller no. 1.5 glass coverslip, and double-sided tape to create a ~20-μl chamber. Approximately 1 μM His_6-KIF15-N700 or KIF18A-N480-GFP-His_6 was incubated in the chamber for 3 min. The chamber was washed with 60 μl wash buffer (WB; 1× BRB80, 1 mM MgATP, and 0.5 mg/ml casein) and then incubated with 1% Pluronic F-127 for 1 min to passivate the surface. The chamber was again washed with 60 μl WB and then incubated with 0.5–1 μM Alexa Fluor 594–labeled MTs (1:10, labeled/unlabeled tubulin) for 3 min. The chamber was then washed with 60 μl flow cell buffer with or without GST-KBP (WB plus 70 mM β-ME, 0.035 mg/ml catalase, 0.2 mg/ml glucose oxidase, and 4.5 mg/ml glucose) and then imaged by epifluorescence microscopy. Time-lapse sequences spanned 2 min with acquisitions captured every 2 s. ImageJ was used for image analysis, and MT velocity was calculated by measuring the distance the MT traveled in total during the 2 -min movie (120 s). The average velocity of control slides from one experimental day was calculated and used to calculate the percent inhibition using the following equation:

$$\%Inhibition = 100 - \left[\left(\frac{Vx}{V\mu} \right) \times 100 \right],$$

where Vx is the velocity of a single MT and $V\mu$ is the average velocity of control MTs from that experimental day.

Co-pelleting assays

MT co-pelleting was performed by incubating 700 nM KIF18A-N480-GFP-His_6 or 1 μM His_6-KIF15-N420 with 2 μM GST-KBP in reaction buffer (10 mM K-Hepes, pH 7.7, 50 mM KCl, 10 mM DTT, 1 mM $MgCl_2$, and 20 μM Taxol; Sigma-Aldrich) for 10 min at room temperature to promote their interaction. KIF18A-N480-GFP-His_6, His_6-KIF15-N420, and GST-KBP were clarified by spinning at 90,000 rpm for 10 min at 4°C before use in assay. Next, 1 μM Taxol-stabilized MTs and 1 mM AMPPNP (Sigma-Aldrich) were added to each reaction and incubated at room temperature for 15 min. The reaction was then spun over 150 μl of sucrose cushion (10 mM K-Hepes, pH 7.7, 50 mM KCl, 20 μM Taxol, and 40% wt/vol sucrose) at 60,000 rpm for 20 min at 26°C. 50 μl of supernatant was removed and mixed 1:1 with 2× sample buffer (SB; 1× SB: 50 mM Tris-Cl, pH 6.8, 2% SDS, 6% glycerol, 1% β-ME, and 200 μg/ml bromophenol blue). The remaining supernatant was removed, and the supernatant/cushion interface was washed twice with reaction buffer. The cushion was then removed and the pellet was gently washed with reaction buffer before being resuspended in 100 μl SB. Both supernatant and pellet samples from each reaction was boiled and vortexed, and 30 μl was run on a 10% SDS-PAGE gel. The gel was then stained with Coomassie for ~30 min and destained overnight before imaging. ImageJ was used to quantify the integrated intensity of each protein band. The integrated intensity of the supernatant and pellet lanes for each reaction was combined to give yield a total protein integrated intensity value, which was used to calculate the percentage of protein in the supernatant.

KIF18A-FL-GFP-His_6 and His_6-GFP-KIF15-FL co-pelleting experiments were performed as described above, except proteins were detected using Western blots instead of Coomassie. For KIF18A-FL-GFP-His_6 experiments, 120 nM kinesin and 342 nM GST-KBP was used. For His_6-GFP-KIF15-FL experiments, 135 nM kinesin and 384 nM GST-KBP was used. Blots were cut ~70 kD, and the top portion was probed with rabbit-His (1:1,000; pm032; MBL) and mouse-KBP (1:1,000; H00026128-B01P; Abnova) and the bottom with α-tubulin (DM1α, 1:5,000; ab7291; Abcam).

CoIP assays

Glutathione agarose slurry (Pierce) was washed with binding buffer (BB; 10 mM K-Hepes, pH 7.7, 50 mM KCl, 1 mM DTT, 100 μM ATP, and 0.1% NP-40) and incubated with 250 nM GST-KBP for 1 h at 4°C with rotation. Agarose was then washed three times with BB and incubated with 20 mg/ml BSA for 30 min at 4°C with rotation. Agarose was washed three times with BB and incubated with 50 nM KIF18A-N480-GFP-His_6, KIF18A-FL-GFP-His_6, His_6-KIF15-N420, or His_6-GFP-KIF15-FL for 1 h at 4°C with rotation. Agarose was pelleted and supernatant was removed and saved, and the agarose pellet was resuspended in BB. Agarose was then washed five to ten times in BB. After washing, agarose was resuspended in 1× SB and boiled. Samples were loaded onto a TGX Stain-Free 10% acrylamide gel (Bio-Rad), resolved by SDS-PAGE, and transferred to a PVDF membrane for immunoblotting.

PVDF membranes were blocked with Odyssey blocking buffer (LI-COR Biosciences) diluted 1:1 in PBS for 1 h at RT and

probed with rabbit-His (1:1,000; pm032; MBL) and mouse-KBP (1:1,000; H00026128-B01P; Abnova) overnight at 4°C. Membrane was washed three times for 10 min with PBST and incubated with secondary antibodies conjugated to Alexa Fluor 700 (A-21036; Invitrogen) or IRDye-800 (925-32211; LI-COR) at 1:5,000 for 1 h at RT. Membrane was washed with PBST and PBS, and bound antibodies were detected using an Odyssey fluorescence detection system (Mandel Scientific).

Live-cell imaging
MEM-α media was removed from transfected cells on poly-D-lysine–coated filming dishes (MatTek) and replaced with CO_2-independent imaging media (Gibco) supplemented with 10% FBS and 1% penicillin and streptomycin. Mitotic cells were identified by scanning for GFP-CENP-B fluorescence using the 60× objective and imaged with the 100× objective using 0.5-μm z-stacks every 2 s for ~5 min. After imaging, the XY position of the cell was marked and revisited within an hour of imaging to determine if the cell had divided for quality control. For mCherry- or mCherry-KBP–expressing cells, 0.5-μm z-stacks of the entire cell were taken in TRITC and GFP channels before time course imaging of GFP-CENP-B.

Chromosome alignment and KIF15 localization analysis
Quantification of chromosome alignment was performed as described previously (Stumpff et al., 2012; Kim et al., 2014). Briefly, single focal plane images of metaphase cells were acquired with both spindle poles in focus. The Plot Profile command in ImageJ was used to measure the distribution of ACA-labeled kinetochore fluorescence within a region of interest defined by the length of the spindle with a set height of 17.5 μm. The ACA signal intensity within the region of interest was averaged along each pixel column, normalized, and plotted as a function of distance along the normalized spindle pole axis. These plots were analyzed by Gaussian fits using Igor Pro (Wavemetrics). The FWHM intensity for the Gaussian fit and the spindle length are reported for each cell analyzed. KIF15 localization was performed similarly, but the endogenous KIF15 fluorescence was plotted across the spindle from a projection of five optical sections taken at 0.2-μm intervals and centered on the mid-cell plane. For chromosome hyperalignment quantification in RPE1 cells, the width of the metaphase plate was measured by determining the longitudinal distance between the most distal chromosomes as reported previously (Häfner et al., 2014). Lastly, for comparison with previously published effects of KBP knockdown on chromosome alignment (Brouwers et al., 2017), we analyzed full z-sections through nonarrested metaphase cells and scored for chromosomes off the metaphase plate.

KIF18A line-scan analysis
Fixed and stained cells were imaged at 100× with 0.2-μm z-stacks taken through the full cell. Line scans were manually measured using the α-tubulin and HEC1 fluorescent intensities to identify well-defined and locally isolated kinetochore MTs. The profile intensities for α-tubulin, HEC1, and KIF18A were measured and recorded. Each channel was normalized internally to its highest value. Line scans were aligned in block by peak HEC1 intensity and averaged for each pixel distance. Standard deviations are reported. Statistical comparisons were performed by fitting a linear regression of the accumulation slope (−0.8 μm to 0 μm) and comparing each condition to that of the control siRNA treatment using an F test.

Chromosome oscillation analysis
Live kinetochore movements were tracked and quantified as reported previously (Stumpff et al., 2008, 2012). Briefly, z-slice projections of GFP-CENP-B movies were used to manually track individual kinetochore pairs with the MTrackJ plugin in ImageJ. Only kinetochore pairs near the middle of the cell were tracked; extreme peripheral kinetochore pairs were not included in the analysis. For mCherry-expressing cells, a base cutoff of 1,000 background subtracted fluorescence units was required for inclusion in the dataset. A macro was used to determine the position of the metaphase plate, which automatically fits a line to the thresholded GFP-CENP-B signal in a time-lapse projection. Kinetochore movement parameters were quantified from kinetochore tracks in Igor Pro (Wavemetrics) and reported as the DMP and DAP. Kymographs of GFP-CENP-B movements were created in ImageJ.

Statistical analysis
Unless otherwise indicated, statistical analyses were performed using one-way ANOVA with Tukey's multiple comparisons test when comparing three or more variables or unpaired, two-sided t tests when only two variables were compared. χ^2 analyses were used to compare binary populations. Data distributions were assumed to be normal, but this was not formally tested.

Online supplemental material
Fig. S1 shows endogenous KBP antibody staining in HeLa and RPE1 cells. Fig. S2 shows the effects of KBP knockdown and overexpression in RPE1 cells. Fig. S3 shows the effects of KBP knockdown and overexpression in HeLa cells without MG132 treatment. Fig. S4 shows that KIF14 knockdown does not affect chromosome alignment or spindle length and that KIF15-knockout cells have short spindles with aligned chromosomes. Fig. S5 shows velocity data from gliding assays in Fig. 3 as well as coIP and co-pelleting data from full-length motor constructs and an SDS-PAGE gel of purified proteins used in in vitro assays. Videos 1–4 include example gliding filament movies for KIF15-N700 and KIF18A-N480 with and without KBP. Videos 5–8 show four examples of GFP-CENP-B kinetochore oscillations, one for each condition of control treatments, KBP siRNA, and mCherry-KBP overexpression.

References

Alves, M.M., G. Burzynski, J.M. Delalande, J. Osinga, A. van der Goot, A.M. Dolga, E. de Graaff, A.S. Brooks, M. Metzger, U.L. Eisel, et al. 2010. KBP interacts with SCG10, linking Goldberg-Shprintzen syndrome to microtubule dynamics and neuronal differentiation. *Hum. Mol. Genet.* 19: 3642–3651. https://doi.org/10.1093/hmg/ddq280

Bakhoum, S.F., and D.A. Compton. 2012. Kinetochores and disease: keeping microtubule dynamics in check! *Curr. Opin. Cell Biol.* 24:64–70. https://doi.org/10.1016/j.ceb.2011.11.012

Brooks, A.S., A.M. Bertoli-Avella, G.M. Burzynski, G.J. Breedveld, J. Osinga, L.G. Boven, J.A. Hurst, G.M. Mancini, M.H. Lequin, R.F. de Coo, et al. 2005. Homozygous nonsense mutations in KIAA1279 are associated with malformations of the central and enteric nervous systems. *Am. J. Hum. Genet.* 77:120–126. https://doi.org/10.1086/431244

Brouwers, N., N. Mallol Martinez, and I. Vernos. 2017. Role of Kif15 and its novel mitotic partner KBP in K-fiber dynamics and chromosome alignment. *PLoS One.* 12:e0174819. https://doi.org/10.1371/journal.pone.0174819

Cimini, D., B. Howell, P. Maddox, A. Khodjakov, F. Degrassi, and E.D. Salmon. 2001. Merotelic kinetochore orientation is a major mechanism of aneuploidy in mitotic mammalian tissue cells. *J. Cell Biol.* 153:517–527. https://doi.org/10.1083/jcb.153.3.517

Donato, V., M. Bonora, D. Simoneschi, D. Sartini, Y. Kudo, A. Saraf, L. Florens, M.P. Washburn, M. Stadtfeld, P. Pinton, and M. Pagano. 2017. The TDH-GCN5L1-Fbxo15-KBP axis limits mitochondrial biogenesis in mouse embryonic stem cells. *Nat. Cell Biol.* 19:341–351. https://doi.org/10.1038/ncb3491

Drévillon, L., A. Megarbane, B. Demeer, C. Matar, P. Benit, A. Briand-Suleau, V. Bodereau, J. Ghoumid, M. Nasser, X. Decrouy, et al. 2013. KBP-cytoskeleton interactions underlie developmental anomalies in Goldberg-Shprintzen syndrome. *Hum. Mol. Genet.* 22:2387–2399. https://doi.org/10.1093/hmg/ddt083

Du, Y., C.A. English, and R. Ohi. 2010. The kinesin-8 Kif18A dampens microtubule plus-end dynamics. *Curr. Biol.* 20:374–380. https://doi.org/10.1016/j.cub.2009.12.049

Häfner, J., M.I. Mayr, M.M. Möckel, and T.U. Mayer. 2014. Pre-anaphase chromosome oscillations are regulated by the antagonistic activities of Cdk1 and PP1 on Kif18A. *Nat. Commun.* 5:4397. https://doi.org/10.1038/ncomms5397

Harper, J.W., G.R. Adami, N. Wei, K. Keyomarsi, and S.J. Elledge. 1993. The p21 Cdk-interacting protein Cip1 is a potent inhibitor of G1 cyclin-dependent kinases. *Cell.* 75:805–816. https://doi.org/10.1016/0092-8674(93)90499-G

Jourdain, L., P. Curmi, A. Sobel, D. Pantaloni, and M.F. Carlier. 1997. Stathmin: a tubulin-sequestering protein which forms a ternary T2S complex with two tubulin molecules. *Biochemistry.* 36:10817–10821. https://doi.org/10.1021/bi971491b

Kevenaar, J.T., S. Bianchi, M. van Spronsen, N. Olieric, J. Lipka, C.P. Frias, M. Mikhaylova, M. Harterink, N. Keijzer, P.S. Wulf, et al. 2016. Kinesin-Binding Protein Controls Microtubule Dynamics and Cargo Trafficking by Regulating Kinesin Motor Activity. *Curr. Biol.* 26:849–861. https://doi.org/10.1016/j.cub.2016.01.048

Kim, H., C. Fonseca, and J. Stumpff. 2014. A unique kinesin-8 surface loop provides specificity for chromosome alignment. *Mol. Biol. Cell.* 25: 3319–3329. https://doi.org/10.1091/mbc.e14-06-1132

Maliga, Z., M. Junqueira, Y. Toyoda, A. Ettinger, F. Mora-Bermúdez, R. W. Klemm, A. Vasilj, E. Guhr, I. Ibarlucea-Benitez, I. Poser, et al. 2013. A genomic toolkit to investigate kinesin and myosin motor function in cells. *Nat. Cell Biol.* 15:325–334. https://doi.org/10.1038/ncb2689

Mayr, M.I., S. Hümmer, J. Bormann, T. Grüner, S. Adio, G. Woehlke, and T.U. Mayer. 2007. The human kinesin Kif18A is a motile microtubule depolymerase essential for chromosome congression. *Curr. Biol.* 17: 488–498. https://doi.org/10.1016/j.cub.2007.02.036

Mayr, M.I., M. Storch, J. Howard, and T.U. Mayer. 2011. A non-motor microtubule binding site is essential for the high processivity and mitotic function of kinesin-8 Kif18A. *PLoS One.* 6:e27471. https://doi.org/10.1371/journal.pone.0027471

Nath, S., D. Ghatak, P. Das, and S. Roychoudhury. 2015. Transcriptional control of mitosis: deregulation and cancer. *Front. Endocrinol. (Lausanne).* 6:60. https://doi.org/10.3389/fendo.2015.00060

Peris, L., M. Wagenbach, L. Lafanechère, J. Brocard, A.T. Moore, F. Kozielski, D. Job, L. Wordeman, and A. Andrieux. 2009. Motor-dependent microtubule disassembly driven by tubulin tyrosination. *J. Cell Biol.* 185: 1159–1166. https://doi.org/10.1083/jcb.200902142

Prosser, S.L., and L. Pelletier. 2017. Mitotic spindle assembly in animal cells: a fine balancing act. *Nat. Rev. Mol. Cell Biol.* 18:187–201. https://doi.org/10.1038/nrm.2016.162

Reinemann, D.N., E.G. Sturgill, D.K. Das, M.S. Degen, Z. Voros, W. Hwang, R. Ohi, and M.J. Lang. 2017. Collective Force Regulation in Anti-parallel Microtubule Gliding by Dimeric Kif15 Kinesin Motors. *Curr. Biol.* 27: 2810–2820.e2816. https://doi.org/10.1016/j.cub.2017.08.018

Safer, D., M. Elzinga, and V.T. Nachmias. 1991. Thymosin beta 4 and Fx, an actin-sequestering peptide, are indistinguishable. *J. Biol. Chem.* 266: 4029–4032.

Sigal, A., R. Milo, A. Cohen, N. Geva-Zatorsky, Y. Klein, Y. Liron, N. Rosenfeld, T. Danon, N. Perzov, and U. Alon. 2006. Variability and memory of protein levels in human cells. *Nature.* 444:643–646. https://doi.org/10.1038/nature05316

Stumpff, J., G. von Dassow, M. Wagenbach, C. Asbury, and L. Wordeman. 2008. The kinesin-8 motor Kif18A suppresses kinetochore movements to control mitotic chromosome alignment. *Dev. Cell.* 14:252–262. https://doi.org/10.1016/j.devcel.2007.11.014

Stumpff, J., Y. Du, C.A. English, Z. Maliga, M. Wagenbach, C.L. Asbury, L. Wordeman, and R. Ohi. 2011. A tethering mechanism controls the processivity and kinetochore-microtubule plus-end enrichment of the kinesin-8 Kif18A. *Mol. Cell.* 43:764–775. https://doi.org/10.1016/j.molcel.2011.07.022

Stumpff, J., M. Wagenbach, A. Franck, C.L. Asbury, and L. Wordeman. 2012. Kif18A and chromokinesins confine centromere movements via microtubule growth suppression and spatial control of kinetochore tension. *Dev. Cell.* 22:1017–1029. https://doi.org/10.1016/j.devcel.2012.02.013

Sturgill, E.G., and R. Ohi. 2013. Kinesin-12 differentially affects spindle assembly depending on its microtubule substrate. *Curr. Biol.* 23: 1280–1290. https://doi.org/10.1016/j.cub.2013.05.043

Sturgill, E.G., D.K. Das, Y. Takizawa, Y. Shin, S.E. Collier, M.D. Ohi, W. Hwang, M.J. Lang, and R. Ohi. 2014. Kinesin-12 Kif15 targets kinetochore fibers through an intrinsic two-step mechanism. *Curr. Biol.* 24: 2307–2313. https://doi.org/10.1016/j.cub.2014.08.022

Sturgill, E.G., S.R. Norris, Y. Guo, and R. Ohi. 2016. Kinesin-5 inhibitor resistance is driven by kinesin-12. *J. Cell Biol.* 213:213–227. https://doi.org/10.1083/jcb.201507036

Tanenbaum, M.E., L. Macůrek, A. Janssen, E.F. Geers, M. Alvarez-Fernández, and R.H. Medema. 2009. Kif15 cooperates with eg5 to promote bipolar spindle assembly. *Curr. Biol.* 19:1703–1711. https://doi.org/10.1016/j.cub.2009.08.027

van Heesbeen, R.G., M.E. Tanenbaum, and R.H. Medema. 2014. Balanced activity of three mitotic motors is required for bipolar spindle assembly and chromosome segregation. *Cell Reports.* 8:948–956. https://doi.org/10.1016/j.celrep.2014.07.015

Vladimirou, E., N. Mchedlishvili, I. Gasic, J.W. Armond, C.P. Samora, P. Meraldi, and A.D. McAinsh. 2013. Nonautonomous movement of chromosomes in mitosis. *Dev. Cell.* 27:60–71. https://doi.org/10.1016/j.devcel.2013.08.004

Weaver, L.N., S.C. Ems-McClung, J.R. Stout, C. LeBlanc, S.L. Shaw, M.K. Gardner, and C.E. Walczak. 2011. Kif18A uses a microtubule binding site in the tail for plus-end localization and spindle length regulation. *Curr. Biol.* 21:1500–1506. https://doi.org/10.1016/j.cub.2011.08.005

Wordeman, L., M. Wagenbach, and G. von Dassow. 2007. MCAK facilitates chromosome movement by promoting kinetochore microtubule turnover. *J. Cell Biol.* 179:869–879. https://doi.org/10.1083/jcb.200707120

Wozniak, M.J., M. Melzer, C. Dorner, H.U. Haring, and R. Lammers. 2005. The novel protein KBP regulates mitochondria localization by interaction with a kinesin-like protein. *BMC Cell Biol.* 6:35. https://doi.org/10.1186/1471-2121-6-35

Xiong, Y., G.J. Hannon, H. Zhang, D. Casso, R. Kobayashi, and D. Beach. 1993. p21 is a universal inhibitor of cyclin kinases. *Nature.* 366:701–704. https://doi.org/10.1038/366701a0